Microstructure and mechanical properties of HfBx coatings deposited on cemented carbide substrates by HiPIMS and DCMS

Haisheng Lin, Chengyong Wang, Zhiwei Lai, Tongchun Kuang, Mohamed Abdou Djouadi

Microstructure and mechanical properties of HfB_x coatings deposited on cemented carbide substrates by HiPIMS and DCMS

Haisheng Lin[a], Chengyong Wang[a], Zhiwei Lai[a], Tongchun Kuang[c], Mohammed Abdou Djouadi[b]*

[a] School of Electromechanical Engineering, Guangdong University of Technology, NO. 100 Waihuan Xi Road, Higher Education Mega Center, Panyu District, Guangzhou, 510006, China.

[b] Institut des Matériaux Jean Rouxel, Université de Nantes, CNRS, 2 Rue de la Houssinière, BP 32229, 44322, Nantes cedex 3, France

[c] School of Materials Science and Engineering, South China University of Technology, 381 Wushan Road, Tianhe District, Guangzhou, P.R.China, 510641

[*]Authors for correspondence.

E-mail:lhs1011@qq.com (Haisheng Lin); cywang@gdut.edu.cn (Chengyong Wang)

Abstract

HfB_x coatings were deposited on cemented carbide substrates by direct current magnetron sputtering (DCMS) and high-power impulse magnetron sputtering (HiPIMS). The effect of the deposition conditions, i.e., temperature, bias voltage and gas pressure, on the crystal structure and mechanical properties of HfB_x coatings were analyzed systematically. The results show that DCMS-deposited HfB_x has random orientations of HfB_2(001), (100), (101) and (102), whereas HiPIMS-deposited one has less random orientations with high intensity in HfB_2(001). Higher temperature, higher bias voltage and lower gas pressure lead to HfB_x coating with stronger HfB_2(001)-preferred orientation because of higher adatom mobility. The DCMS-deposited HfB_x coatings have a columnar microstructure and rough surface morphology. In contrast, the HiPIMS-deposited HfB_x coatings have an extremely dense microstructure and smooth surface, mainly due to high ion bombardment. Attributing to high crystallinity and high density, HfB_x coatings deposited by HiPIMS have superhardness up to 49.3 ± 3.6 GPa and high Young's modulus of 667.0 ± 9.2 GPa. DCMS-deposited HfB_x, on the other hand, have a much lower hardness between 27.3 ± 4.2 and 36.3 ± 2.5 GPa. Moreover, excellent adhesion (> 100 N) of HfB_x coating on the cemented carbide substrate can be obtained, originating from the chemical diffusion and the mechanical locking in the interface.

Keywords: HfB_2 coating, magnetron sputtering, Microstructure, Hardness, Adhesion

1. Introduction

Hafnium diboride (HfB_2) is a well-known ultra-high-temperature ceramic (UHTC) with a hexagonal structure. HfB_2 has excellent physical properties, including a high melting point (3380 °C), high bulk hardness (28 GPa), high thermal conductivity (>100 $W\cdot(m\cdot K)^{-1}$), low thermal expansion ($6.3x10^{-6}K^{-1}$) and good corrosion resistance [1-3]. The lattice mismatch between HfB_2 and GaN [4] is only 1.4%, suggesting that HfB_2 is possibly an ideal buffer layer for the growth of semiconductors. Therefore, HfB_2 coating is considered to have a high potential to be used in aerospace [5,6], thermophotovoltaic devices [7], complementary metal oxide semiconductors (CMOS) [8], and cutting tools. Hence, the study on the growth of high-quality HfB_2 coating has excellent scientific and technological importance.

Obtained by chemical vapor deposition (CVD) from single-source precursor $Hf(BH_4)_4$ [9-11], the texture of HfB_2 film is greatly dependent on the substrates like Si(111), Si(001), c-Si, SiO_2, and deposition temperatures which are usually in the range of 400-900 °C [9] and pressure [10]. Epitaxial HfB_2 (0001) was grown on Si (001) substrate at a high temperature of 1000 °C by etching through a SiO_2 layer [15]. For the HfB_x (x value is higher or lower than 2) coating deposited by radio frequencies magnetron sputtering (RFMS) [12-14], its crystallization could be adjusted from the amorphous, cluster, poor pronounced columnar to columnar, with the variation of bias voltage and temperature simultaneously [12]. The corresponding hardness can be increased from 13 GPa for the amorphous film to 44 GPa for the (001) preferred oriented film [12]. A recent publication reported that the HfB_2 coating deposited by DCMS on the Al_2O_3 substrate presents a hardness of 47.7 ± 2.7 GPa [16]. Moreover, HfB_2 coating was deposited on stainless steel by DCMS with Al_2O_3 coating as a top layer [17]. This HfB_2/Al_2O_3 solar absorber coating was thermally stable in vacuum at 600 °C for 2 h, indicating that HfB_2 could be a potential material for high-temperature solar thermal applications. Bakhit B et al. [18] reported the synthesis of dense Ti0.67Hf0.33B1.7 thin film with a hardness of ~41.0 GPa grown without external heating by hybrid HiPIMS and DCMS co-sputtering (HfB_2-HiPIMS/TiB_2-DCMS) on Al_2O_3 substrates. To the best of our knowledge, there are no reports on the deposition of HfB_x coatings, including stoichiometric and off-stoichiometric compositions, on the cemented carbide substrate (WC/Co) as coated cutting tools. In addition, microstructure and mechanical properties of HfB_x coatings deposited by magnetron sputtering technology, especially HiPIMS, also

require further investigation.

In this paper, we adopted direct current magnetron sputtering (DCMS) and high-power impulse magnetron sputtering (HiPIMS) to deposit HfB_x coating on cemented carbide substrates. The influence of different deposition parameters on the microstructure and mechanical properties of HfB_x coating were studied. Furthermore, the adhesion mechanism between HfB_x coating and cemented carbide was explored.

2. Experimental methods

2.1 Coating deposition

HfB_x coatings were deposited on the mirror-polished (Ra < 0.04 μm) substrate of YL10.2 cemented carbide (manufacturer: ZCC·CT). Before the deposition, all the samples were ultrasonically cleaned and dried. The industrial-scale physical vapor deposition (PVD) equipment Domino Mini from Sulzer Metaplas, which is equipped with arc-enhanced glow discharge (AEGD), dcMS and HiPIMS technologies, was used for the deposition. The etching process with AEGD using a Ti target with 99.99 % purity was executed prior to the deposition of the coatings. The background pressure was evacuated to less than 4.0×10^{-3} Pa before the deposition. HfB_2 compound target (manufacturer: Plansee) was used to prepare coatings. The HfB_2 target is 456 mm in length, 81 mm in width and 5 mm in thickness, and the purity of the target is 99.9 %. Magnets were mounted in a closed field configuration behind the target, and the effective coating area was 400 mm in length. Only one magnetron was used, and the samples were mounted in front of it. The minimum distance between sample and target is 87 mm. The working gas Ar had high purity of 99.999 %. The deposition conditions for different samples prepared using DCMS and HiPIMS are listed in Tables 1 and 2, respectively. High power magnetron sputtering power supply was used in power control mode, with an average power of 4 kW. The monitoring screen showed that the discharge voltage and average current values were about 800 V and 5 A, respectively. The peak power was calculated to be 140 kW.

2.2 Characterization

A Bruker D8 Advance X-ray Diffractometer, with Cu K_α source and wavelength λ = 0.154 nm, was used to measure the phase structures and orientations of HfB_x

coatings. Hitachi SEM S-3400N-II acquired the surface morphology and cross-section structure of HfB_x coatings. The acceleration energy of 15 kV was applied. To observe the cross-section structure of the coating, wire cutting was used to cut the coating samples from the cross-sectional direction. Bruker AFM Dimension FastScan Microscope was utilized to measure the 3D topology of the coating with the scanning area of 1 um×1 um. The microstructures of the HfB_x coatings were observed by field-emission transmission electron microscopy (Thermo Fisher Scientific Talos F200S of FEI) with an EDS and an accelerating voltage of 200 kV. The sample used for transmission electron microscopy (TEM) detection was prepared by the focus ion beam. The surface chemical bonding states and the composition of the coatings were investigated using the X-ray photoelectron spectroscopy (XPS) with an Escalab 250Xi XPS Spectrometer (Thermo Fisher, USA). High-resolution spectra were acquired with a 0.1 eV step with a pass energy of 20 eV, corresponding to an overall Fermi edge resolution of 0.39 ± 0.02 eV. The binding energy of C1s (285.0 eV) was used to calibrate the energy scale of the spectra. A Shirley background subtraction method was beneficial in analyzing to differentiate the XPS peaks. Concerning the mechanical properties, Nano Indenter XP^{TM} from Anton Paar was used to measure the hardness and Young's modulus of the coatings, with a depth of indention of 100 nm, dwelling time of 3 s and an applied load of 10 mN. Berkovich diamond indenter was used, with 25 indents per sample for nanoindentation measurement. The scratch tester RST from Anton Paar was used to evaluate the adhesion of HfB_x coatings on cemented carbide substrates, with scratch loads ranging from 0 to 100 N, scratch length of 5 mm, and scratch speed of 10 mm/min. Rockwell indenter with a radius of 0.2 mm was used for the scratch measurement.

3. Results and discussion

3.1 Crystallinity and microstructure

The x-ray diffraction pattern of HfB_x coatings deposited by DCMS is shown in Fig. 1. Heating temperature and bias voltage were changed and the corresponding XRD patterns were obtained. The peak around 24.5° is assigned to HfB_2 with (001) orientation, and it has the highest intensity relative to all the other peaks. Peaks from HfB_2(100), (101), (002) and (102) orientations are also found and marked in Fig. 1, which indicate the polycrystalline nature of the HfB_x coatings. With the increase of bias voltage from -50 to -200 V at a heating temperature of 600 °C, the peak intensity associated with (001) orientation becomes higher. In addition, the peak intensity

associated with (001) orientation corresponding to a low heating temperature (500 °C) and a high bias voltage (-150 V) is lower than the peak intensity corresponding to a high temperature (600 °C) but a low bias voltage (-100 or 50 V). It implies that heating temperature and bias voltage are critical factors for the crystallinity of HfB_x coatings with (001)-preferred orientation using DCMS. It is also consistent with the growth principle of the coatings proposed in the literature [19].

Figure 2 shows the XRD pattern of HfB_x coatings deposited by HiPIMS with different bias voltages and argon gas pressure. It can be found that the highest peak of the HfB_2 in the XRD pattern corresponds to the (001) orientation. Unlike the XRD pattern of HfB_x coating deposited by DCMS, fewer peaks can be observed from other orientations in the XRD pattern of HfB_x coatings deposited by HiPIMS. The HfB_x coatings with HfB_2(001) orientation and a bias voltage of -100 V possess a peak at 25.0°. The same peak shifts to 25.17° with a bias voltage of -200 V. The shift of the peak indicates higher compressive stress of the HfB_x coating. It is due to stronger ion bombardment on the coating surface because of higher bias voltage. No noticeable difference in the intensity of (001) orientation peaks can be observed for different bias voltages regarding HfB_x coatings deposited by HiPIMS.

Moreover, when the working pressures of argon gas changed from 0.65 to 0.5 Pa, a change in intensity and slight shift of the angle to 25.22° of (001) orientation peaks can be found. Lower working pressure contributes to a smaller mean free path and reduced energy loss by the collision of particles in plasma. Particles reaching the surface of the coating with higher kinetic energies induce better growth of HfB_2 grains.

The cross-sectional high-resolution transmission electron microscope (HRTEM) shows that the DCMS-deposited HfB_x coatings possess multiple orientations like HfB_2(001), (100), (101) and others, indicating the polycrystalline nature of the coating. Moreover, the HiPIMS-deposited HfB_x coating crystals are highly oriented in the HfB_2(001) orientation along the *c* axis. Likewise, the nanocolumnar structure along the direction of growth of the coating is also found and shown in Fig. 3(b).

HfB_x coating with HfB_2(001)-preferred oriented can be obtained regardless of the sputtering methods like DCMS, HiPIMS and RFMS [20]. The texture evolution of HfB_x coatings can be explained by adatom surface diffusion [21], which occurs among planes and among grains during the initial or growth stages of the surface of films [22]. It greatly influenced the texture evolution of other transition metal

diborides like TiB_2 [23] and CrB_2 [24]. According to the theory reported in [22], in the case of low surface adatom mobility, grains on the plane that has lower surface diffusivity parallel to the substrate survive and become the preferred orientation. However, at higher surface adatom mobility and longer diffusion distances, diffusion among grains occurs and grains with the lowest-surface-energy plane become the preferred orientation.

Concerning hexagonal HfB_2 (*h*-HfB_2), Zhang et al. calculated the surface energy, with thermodynamic sense of several HfB_2 surfaces, including (0001), $(10\bar{1}0)$, $(10\bar{1}1)$ and $(10\bar{2}3)$. They found that Hf-terminated (0001) surface and B-terminated (0001) surface have the lowest surface formation energy at the Hf-rich area and B-rich end area, respectively [25]. At higher deposition temperatures, atoms gain more thermal energy and consequently have higher adatom mobility. The growing coating surface gains additional energy from high ion bombardment by increasing bias voltage. Consequently, the coating favors the growth of the lowest-surface-energy orientation (001). Due to this reason, a highly HfB_2(001)-oriented coating is obtained after using high deposition temperature and bias voltage in DCMS. Compared to DCMS, HiPIMS-deposited HfB_x coating exhibits a higher intensity of the peak associated with (001) orientation, but has fewer peaks assigned to other orientations. It is because of the continuous ion bombardment on the coating surface from the high ionization rate of HiPIMS [26]. It leads to high surface adatom mobility [27] and highly HfB_2(001)-oriented HfB_x coating.

3.2 Surface and cross-sectional morphology

SEM and AFM were used to observe the cross-sectional view, surface morphology and 3D-topology of different HfB_x coatings deposited by DCMS and HiPIMS, as shown in Fig. 4 and 5.

HfB_x coatings deposited by DCMS, with different deposition conditions, have a prominent columnar cross-sectional structure, which is of coarse and have low density. On the other hand, all HfB_x coatings deposited by HiPIMS show a highly compact and smooth structure without macro features.

Based on the surface observed by SEM and AFM, HfB_x coatings deposited by DCMS have small spherical islands. Their arrangement on the surface is random with non-uniform size. Some small "islands" get together to form an "island clusters", and a clear boundary of among "island clusters" can be observed. However, HfB_x coatings deposited by HiPIMS have an extremely smooth surface, and no particles can be

observed in the magnified view, as shown in Fig. 5.

HfB_x coatings with significantly different morphologies were obtained by DCMS and HiPIMS. Due to the high ionization and high peak power density in HiPIMS, surface adatom mobility is greatly improved compared to conventional DCMS technology, resulting in a dense and uniform structure. In addition, high ion bombardment in HiPIMS contributes to grain refining and prevents from the columnar structure formation .

3.3 Mechanical properties

Hardness and Young's modulus of HfB_x coatings deposited by DCMS are shown in Fig. 6. For the coatings deposited at low heating temperature (500 °C), relatively low hardness and Young's modulus are measured with values of 27.3 ± 4.2 and 470.5 ± 6.6 GPa, respectively. It is because of the low crystallinity of the coatings. For the HfB_x coatings deposited at higher heating temperature (600 °C), with the increase of bias voltage from -50 to -200 V, the hardness increases slightly from about 33.4 ± 2.2 to 36.3 ± 2.5 GPa. For the same increase of bias voltage, Young's modulus increases from 470.5 ± 6.6 to 567.4 ± 8.1 GPa. It is due to higher ion bombardment on the coating surface during the deposition and formation of a structure with higher crystallinity, as shown in the XRD results in Fig. 1.

Considering the deposition by HiPIMS, all the HfB_x coatings have superhardness (≥ 40 GPa), illustrated in Fig. 7. By increasing the bias voltage from -100 to -200 V (at working pressure 0.6 Pa), the hardness and Young's modulus can be increased from 42.6 ± 3.8 to 45.1 ± 2.5 GPa, and 571.8 ± 8.9 to 583.0 ± 7.0 GPa, respectively. Additionally, on decreasing the working pressure from 0.65 to 0.5 Pa, the hardness and Young's modulus of HfB_x coating further increase from 45.1 ± 2.5 and 583.0 ± 7.0 GPa to 49.3 ± 3.6 and 667.0 ± 9.2 GPa, respectively. The different values of hardness for HfB_x coatings under different conditions are consistent with the crystallinity, as per the XRD results shown in Fig. 2.

From the first principle calculations, *h*-HfB_2 is a material of hard nature with a calculated Vickers hardness of 40.7 GPa [29] and the weakest ideal strength of 33.3 GPa [30]. Note that the theoretically calculated bulk hardness is based on the ideal crystal structure of *h*-HfB_2. The mechanical properties of the experimentally deposited coatings are greatly influenced by crystallinity and microstructure when deposited by different processes. For example, a previous study [31] reported that nanoindentation

revealed 15 GPa higher hardness of (0001)-oriented *h*-WB_2 coating as compared to the (1011)-orientated one.

According to the hardness measuring results in this study, HfB_x coating can be hard or even superhard. As for the coatings deposited by HiPIMS, the ion flux is much larger than other sputtering methods, such as DCMS and middle-frequency pulsed MS [28]. High atomic mobility can be induced by bombarding the growing coating with energetic heavy Hf+ ions generated by HiPIMS sputtering of the HfB_2 target [18]. According to the present study, the deposition rate of the HiPIMS-deposited HfB_x coating (about 5 nm/min) is much lower than the DCMS-deposited one (about 11~14 nm/min). When HiPIMS is used, the coating structure is dense and has no micro features, and the coatings would have higher crystallinity in (001) orientation as compared to DCMS. HfB_x coatings deposited by DCMS have low crystallinity, random orientations and coarse columnar structure, due to the fast deposition rate and insufficient energy of particles upon reaching the coating surface. Therefore, the coatings prepared by HiPIMS exhibits higher hardness than those prepared by DCMS.

In order to explore the effect of the composition ratio in HfB_x coating on the mechanical properties of the coating, high-resolution XPS B1s spectra of HfB_x coatings was observed, as shown in Fig. 8. The peaks at about 192.1, 187.75 and 186.7 eV are attributed to B in the B_2O_3 [37], HfB_2 [35] and metallic boron [38-41] respectively. Note that air-exposed samples were used for the measurement and sputtering process was avoided. It was because of the risk of preferential removal or implantation of low atomic mass species (boron) by sputtering, making accurate phase identification difficult (impossible). Although most TMB_2 coatings are over-stoichiometric [32-34], some have been reported to be under-stoichiometric [42,43]. However, the presence of the B-B peak in XPS indicates that these HfB_x coatings are indeed over-stoichiometric. Possible reasons, which need to be verified, may include the longer mean free path of the B atom than the Hf atom, or the much higher mass of Hf compared to Ar resulting in slight deflection of Hf. In the study of the compositional evolution of Ti-B thin films deposited by sputtering a compound target, Neidhardt J et al. found that the coatings composition Ti/B ratio mainly

depends on gas pressure, target-substrate distance and angle [44]. HfB_x coatings, with constituents with a large difference in atomic mass or radius, may also have similar laws of influence [44], and further research studies are needed to verify.

The B-B/B-Hf ratios is calculated from the area of B1s spectra, as shown in Fig. 9. The calculated results show that the B-B/B-Hf ratio of HiPIMS-deposited coating is higher than that deposited by DCMS. Considering the higher hardness of HiPIMS-deposited HfB_x coatings as compared to that deposited by DCMS, a higher amount of boron may be associated with higher hardness.

The mechanism of the enrichment or deficiency of the boron phase on the hardening of the HfB_x coating needs further deep investigation. The contribution of B-B bonding from B1s spectra was assigned to the thin B-tissue phase encapsulating the TiB_2 nanocrystals observed by TEM [39]. In the present study of HfB_x coatings, a similar structure to the TiB_2 coating with B-enrichment [32] was observed by HRTEM (Fig. 3). Excess B phase tissue along the TMB_2 column was also found from the study of other TMB_2 coatings, i.e., TiB_2 [32], CrB_2 [33] and VB_2 [34]. Mayrhofer et al. [32] and N. Kalfagiannis et al. [36] associated the hardening effect of the coating with the formation of these B phases. It is reported that higher crystallinity in (001) orientation for RFMS-deposited HfB_x coating has a higher amount of B/Hf ratio and higher hardness [12]. HfB_x coatings might also be under-stoichiometric. In the case of under-stoichiometric TMB_x [42,43], recent publication reports that deficiency of B in under-stoichiometric HiPIMS-deposited $TiB_{1.43}$ film is found to be accommodated by Ti-rich planar defects, and the film exhibit a superior hardness of 43.9 ± 0.9 GPa [43].

The scratch on the surface of the DCMS-deposited coating is shown in Fig. 10a. Minimal chipping of the coating suddenly occurs at the side of the scratch track at the critical load of 78.5 N. No apparent delamination or chipping of the coating from the surface can be observed with scratching from 0 to 100 N, indicating excellent adhesion of the coating to the substrate.

As shown in Fig. 10b, there is no cohesive failure (i.e., failure of the coating before delamination) on the surface of HiPIMS-deposited coating under the scratch loads from 0 to 100 N, suggesting excellent adhesion strength of the coating. Tiny localized hemispherical chipping of the coating begins to appear at the side of the

track at the critical load of 55 N. However, the coating removal inside the scratch track exacerbates smoothly with the load. It is in contrast to the DCMS-deposited coating, where chipping of the coating occurs suddenly. It is due to higher damage resistance and higher hardness of the coating deposited by HiPIMS.

In order to profoundly investigate the adhesion behavior between the coating and cemented carbide (WC/Co) substrate from a microscopic view, HRTEM was conducted to observe the interface, as shown in Fig. 11 and 12. The HfB_x coating was deposited directly on the substrate without a buffer layer. Figure 11 shows the interface of HfB_x coating and WC grains. The coating and the WC grain are perfectly connected. EDS was also conducted on the interface, and the inset in Fig. 11 is the line-scan EDS signal scanned from the coating toward the substrate. It is found that both of the heavy elements Hf and W have gradient diffusion towards the other side. The WC grains are followed by a thin amorphous layer of 2–3 nm thickness before the formation of HfB_2 crystals. It can also be observed that the crystallinity of HfB_2 is low at the start of the nucleation stage.

Due to the etching on the surface of the cemented carbide substrate before deposition and different etching rates of WC grains and Co phases, a larger amount of Co is removed than WC grains. Therefore, a “nano-rough” surface with Co phases at lower positions is obtained. The growth of coating in such an area with surfaces of different heights contributes to the mechanical “locking” of the coating, as shown in Fig. 12, and improves the adhesion of the coating on the substrate.

Consequently, element diffusion and mechanical “locking” on the interface lead to excellent adhesion of HfB_x coating on cemented carbide substrate.

4. Conclusion

In this study, HfB_x coatings were deposited on cemented carbide substrate using DCMS and HiPIMS. The effects of the deposition process on the crystal structure, coating morphology and mechanical properties were analyzed, leading to the following results.

Higher heating temperature, higher bias voltage and lower working gas pressure, contribute to more thermal energy and kinetic energy on the surface, leading to higher adatom mobility and HfB_x coating with stronger HfB_2(001)-preferred orientation. Moreover, high ion bombardment of HiPIMS results in the refining of grains, dense cross-sectional microstructure without obvious micro-feature, and smooth surface

morphology, whereas the dcMS deposited HfB_x coating has a columnar structure and surface morphology with small non-uniform spherical-like islands.

For both sputtering methods, the hardness of HfB_x coatings increases with crystallinity. HiPIMS-deposited HfB_x coatings possess a maximum superhardness up to a value of 49.3 ± 3.6 GPa. It is because of the coating's hard nature and high crystallinity. The excellent adhesion strength of the coatings on the cemented carbide substrates, without cohesive failure, can be obtained for both DCMS and HiPIMS methods. Further investigation reveals that such an excellent adhesion strength originated from the thin amorphous layer with diffusing elements in the interface and the mechanical locking due to the step structure among coating, WC, and Co grains.

Declaration of Competing Interest

The authors declare that they have no known competing financial interests or personal relationships that could have appeared to influence the work reported in this paper.

Acknowledgments

This work was supported by the National Natural Science Foundation of China Youth Project (Grant no. 52005111).

References

[1] Zhang L, Pejaković D A, Marschall J, et al. Thermal and Electrical Transport Properties of Spark Plasma-Sintered HfB_2 and ZrB_2 Ceramics[J]. Journal of the American Ceramic Society, 2011, 94(8): 2562-2570.

[2] Gasch M, Johnson S, Marschall J. Thermal conductivity characterization of hafnium diboride-based ultra-high-temperature ceramics[J]. Journal of the American Ceramic Society, 2008, 91(5): 1423-1432.

[3] Fahrenholtz W G, Hilmas G E, Talmy I G, et al. Refractory Diborides of Zirconium and Hafnium[J]. Journal of the American Ceramic Society, 2007, 90(5):18.

[4] Yamada-Takamura Y, Wang Z T, Fujikawa Y, et al. Surface and interface studies of GaN epitaxy on Si(111) via ZrB_2 buffer layers[J]. Physical Review Letters, 2005, 95(26):266105.

[5] Upadhya K, Yang J M, Hoffman W P. Advanced materials for ultrahigh temperature structural applications above 2000 °C[J]. Journal of the American Ceramic Society, 1997, 76(12): 51-56.

[6] Squire T H, Marschall J. Material property requirements for analysis and design of UHTC components in hypersonic applications[J]. Journal of the European Ceramic Society, 2010, 30(11): 2239-2251.

[7] Arpin K A, Losego M D, Cloud A N, et al. Three-dimensional self-assembled photonic crystals with high temperature stability for thermal emission modification[J]. Nature communications, 2013, 4: 2630.

[8] Zagozdzon-Wosik W, Darne C, Radhakrishnan D, et al. Applications of metallic borides for gate electrodes in CMOS integrated circuits[J]. Reviews on advanced materials science, 2004, 8(2).

[9] Yang Y, Jayaraman S, Kim D Y, et al. Crystalline texture in hafnium diboride thin films grown by chemical vapor deposition[J]. Journal of Crystal Growth, 2006, 294(2):389-395.
[10]Yang Y, Jayaraman S, Kim D Y, et al. CVD growth kinetics of HfB_2 thin films from the single-source precursor Hf(BH4)(4)[J]. Chemistry of Materials, 2006, 18(21):5088-5096.
[11]Chatterjee A, Kumar N, Abelson J R, et al. Nanoscratch and nanofriction behavior of hafnium diboride thin films[J]. Wear, 2008, 265(5-6):921-929.
[12]Goncharov A A, Agulov A V. Structure, composition, and physicomechanical characteristics of HfB_2 and Hf-B-N films[J]. Physics of Metals and Metallography, 2013, 114(1):95-101.
[13]Eldridge J M, Forouhi A R, Gorman G L, et al. Various properties of sputter-deposited HfB_2 films[J]. Journal of the Electrochemical Society, 1990, 137(12): 3905-3909.
[14]Yu J, Dong L, Li C, et al. The influence of modulation periods on the evolution of microstructure and mechanical properties of nanoscale HfN/HfB_2 multilayers[J]. Surface and Coatings Technology, 2017, 326: 368-374.
[15]Yang Y, Abelson J R. Epitaxial growth of HfB_2 (0001) on Si (001) by etching through a SiO_2 layer[J]. Journal of Crystal Growth, 2008, 310(13): 3197-3202.
[16]Glechner T, Hudak O E, Wojcik T, et al. Influence of the non-metal species on the oxidation kinetics of Hf, HfN, HfC, and HfB2 coatings[J]. Materials & Design, 2021, 211: 110136.
[17]Qiu X L, Gao X H, He C Y, et al. Structure, optical simulation and thermal stability of the HfB2-based high-temperature solar selective absorbing coatings[J]. RSC advances, 2019, 9(51): 29726-29733.
[18]Bakhit B , S Mráz, Lu J , et al. Dense Ti0.67Hf0.33B1.7 thin films grown by hybrid HfB2-HiPIMS/TiB2-DCMS co-sputtering without external heating[J]. Vacuum, 2021, 186(1):110057.
[19]Thornton J A. The microstructure of sputter-deposited coatings[J]. Journal of Vacuum Science & Technology A: Vacuum, Surfaces, and Films, 1986, 4(6): 3059-3065.
[20]Buranich V, Pogrebnjak A, Budzynski P, et al. Mechanical and tribological characterization of nanostructured HfB_2 films deposited from compound target[J]. SN Applied Sciences, 2020, 2(4).
[21]Greene J E, Sundgren J, Hultman L, et al. Development of preferred orientation in polycrystalline TiN layers grown by ultrahigh vacuum reactive magnetron sputtering[J]. Applied Physics Letters, 1998, 67(20):2928-2930.
[22]Kajikawa Y, Noda S, Komiyama H. Comprehensive perspective on the mechanism of preferred orientation in reactive-sputter-deposited nitrides[J]. Journal of Vacuum Science and Technology A Vacuum Surfaces and Films, 2003, 21(6):1943-1954.
[23]Zhang T F, Gan B, PARK, et al. Influence of negative bias voltage and deposition temperature on microstructure and properties of superhard TiB_2 coatings deposited by high power impulse magnetron sputtering[J]. Surface and Coatings Technology, 2014, 253(9):115-122.
[24]Zhang S, Wang Z, Guo P, et al. Temperature induced superhard CrB_2 coatings with preferred (001) orientation deposited by DC magnetron sputtering technique[J]. Surface and Coatings Technology, 2017, 322:134-140.
[25]Y. Zhang, S. Sanvito, First-principles investigation of the thermodynamic stability of MB_2 materials surfaces (M=Ti/Zr/Hf), Journal of the American Ceramic Society 101 (2018) 4118-4127.
[26]A. P. Ehiasarian, Y. A. Gonzalvo, T. D. Whitmore, Time-Resolved Ionisation Studies of the High Power Impulse Magnetron Discharge in Mixed Argon and Nitrogen Atmosphere, Plasma Processes and Polymers 4(2007) 309-313.
[27]Mayrhofer P H, Kunc F, Musil J, et al. A comparative study on reactive and non-reactive unbalanced magnetron sputter deposition of TiN coatings[J]. Thin Solid Films, 2002, 415(1-2):151-159.
[28]Ehiasarian A P, Gonzalvo Y A, Whitmore T D. Time-Resolved Ionisation Studies of the High Power Impulse Magnetron Discharge in Mixed Argon and Nitrogen Atmosphere[J]. Plasma Processes and Polymers, 2007, 4(S1): S309-S313.
[29]Pan Y, Huang H, Wang X, et al. Phase stability and mechanical properties of hafnium borides: A first-principles study[J]. Computational Materials Science, 2015, 109:1-6.
[30]Zhang X, Luo X, Li J, et al. The Ideal Strength of Transition Metal Diborides TMB2 (TM = Ti, Zr, Hf): Plastic Anisotropy and the Role of Prismatic Slip[J]. Scripta Materialia, 2010, 62(8):625-628.

[31]C. Fuger, R. Hahn, L. Zauner, T. Wojcik, M. Weiss, A. Limbeck, O. Hunold, P. Polcik, H. Riedl, Anisotropic super-hardness of hexagonal WB2±z thin films, Mater. Res. Lett. 10 (2022) 70-77.
[32]P.H. Mayrhofer, C. Mitterer, J. Wen, J.E. Greene, I. Petrov, Self-organized nanocolumnar structure in superhard TiB_2 thin films, Applied Physics Letters 86(13) (2005) 131909.
[33]M. Audronis, P.J. Kelly, A. Leyland, A. Matthews, A TEM study of the structure of magnetron sputtered chromium diboride coatings, Journal of Physics: Conference Series. IOP Publishing 26 (2006) 355.
[34]F. Ge, C. Chen, S. Rui, F. Meng, H. Feng, Hard and wear resistant VB_2 coatings deposited by pulsed DC magnetron sputtering, Vacuum 135 (2017) 66-72.
[35]Chowdhury S, Polychronopoulou K, Cloud A, et al. Nanomechanical and nanotribological behaviors of hafnium boride thin films[J]. Thin Solid Films, 2015, 595:84-91.
[36]N. Kalfagiannis, G. Volonakis, L. Tsetseris, S. Logothetidis, Excess of boron in TiB_2 superhard thin films: a combined experimental and ab initio study, J. Phys. D. Appl. Phys. 44 (2011) 385402.
[37]Burke AR, Brown CR, Bowling WC, Glaub JE, Kapsch D, Love CM, Whitaker RB, Moddeman WE. Ignition mechanism of the titanium-boron pyrotechnic mixture. Surface and Interface Analysis. 1988 Apr;11(6-7):353-8.
[38]J. J. Shea, Springer handbook of condensed matter and materials data, IEEE Electrical Insulation Magazine, 22(2006) 49-49.
[39]N. Nedfors, A. Mockute, J. Palisaitis, P. Persson, L. Naslund, J. Rosen, Influence of pulse frequency and bias on microstructure and mechanical properties of TiB_2 coatings deposited by high power impulse magnetron sputtering, Surface & Coatings Technology 304 (2016) 203-210.
[40]HENDRICKSON, David N.; HOLLANDER, Jack M.; JOLLY, William L. Core-electron binding energies for compounds of boron, carbon, and chromium. Inorganic Chemistry, 1970, 9.3: 612-615.
[41]Schreifels JA, Maybury PC, Swartz Jr WE. X-ray photoelectron spectroscopy of nickel boride catalysts: correlation of surface states with reaction products in the hydrogenation of acrylonitrile. Journal of Catalysis. 1980 Sep 1;65(1):195-206.
[42]Hellgren N, Thörnberg J, Zhirkov I, et al. High-power impulse magnetron sputter deposition of TiBx thin films: Effects of pressure and growth temperature. Vacuum, 2019, 169: 108884.
[43]Thörnberg J, Palisaitis J, Hellgren N, et al. Microstructure and materials properties of understoichiometric TiBx thin films grown by HiPIMS. Surface and Coatings Technology, 2020, 404: 126537.
[44]Neidhardt J, Mraz S, Schneider J M, et al. Experiment and simulation of the compositional evolution of Ti-B thin films deposited by sputtering of a compound target. Journal of Applied Physics, 2008, 104(6):377.

Table 1 Deposition conditions of various DCMS-deposited HfB_x coatings

Sample	DC-1	DC-2	DC-3	DC-4
Power (kW)	4			
Ar (sccm)	160			
Pressure (Pa)	0.78			
Bias voltage (V)	-150	-50	-100	-200
Heating temperature (°C)	500	600	600	600
Deposition time (min)	150			

Table 2 Deposition conditions of various HiPIMS-deposited HfB_x coatings

Sample	HiP-1	HiP-2	HiP-3
Average Power (kW)	4		
Ar (sccm)	140		
Pressure (Pa)	0.65	0.65	0.5
Bias voltage (V)	-100	-200	-200
Heating temperature (°C)	600		
On/off (us)	40/1000		
Deposition time (min)	300		

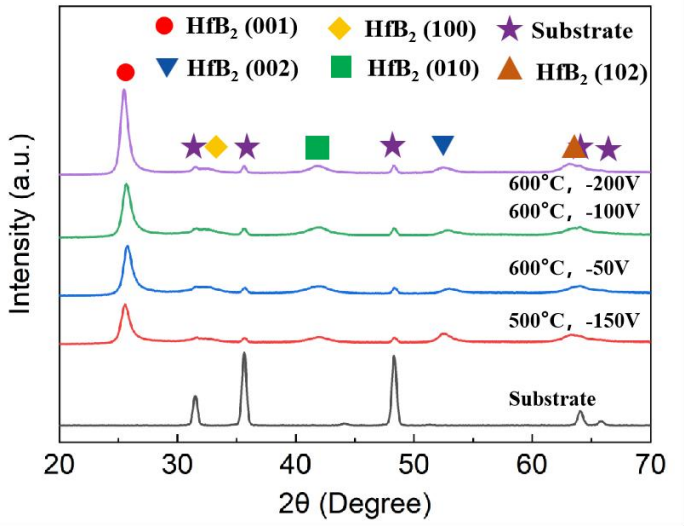

Fig. 1 X-ray diffraction pattern of HfB_x deposited by DCMS (Deposition parameters: 4 kW, 160 sccm Ar, 0.78 Pa.)

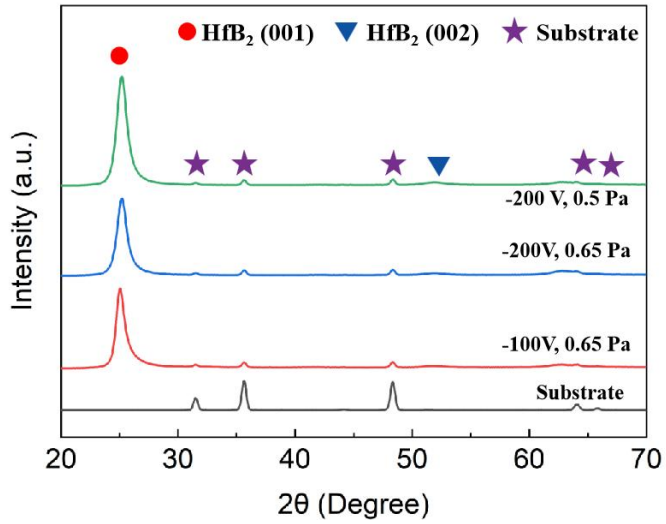

Fig. 2 X-ray diffraction pattern of HfB_x deposited by HiPIMS (Deposition parameters: 4 kW, 600 °C, 40/1000 us.)

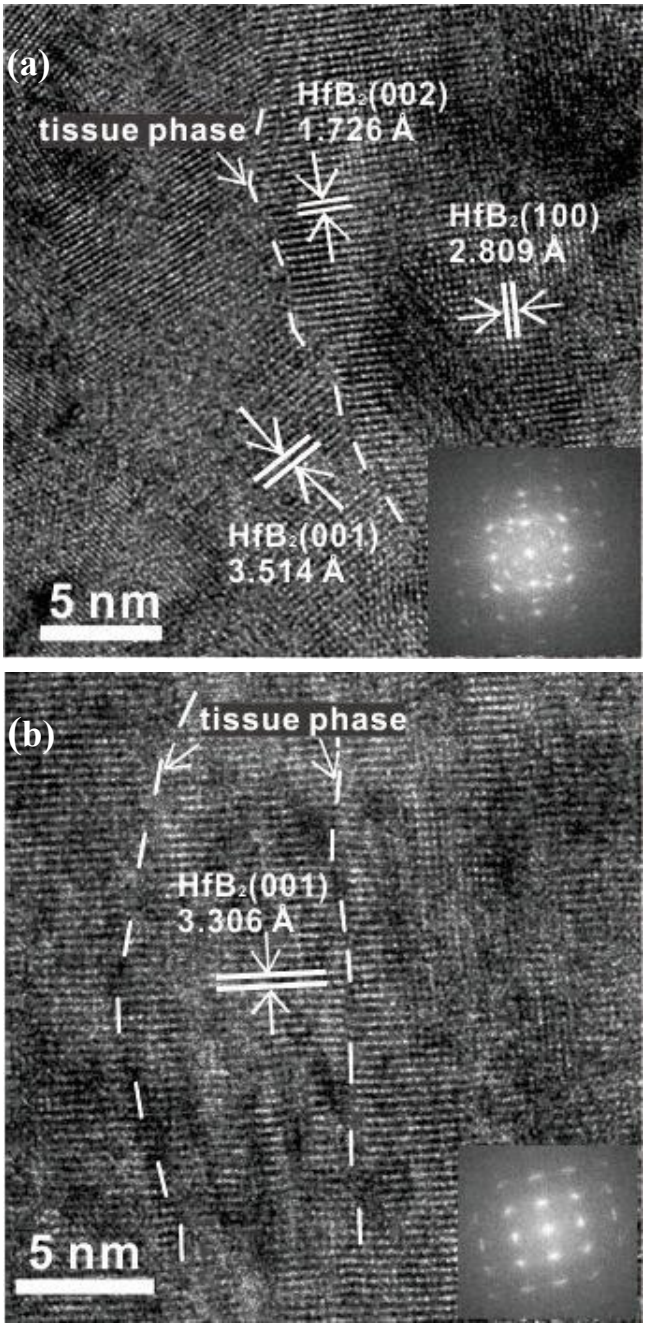

Fig. 3 Microstructure of HfB_x coating deposited by (a)DCMS and (b) HiPIMS (Deposition parameters for DCMS: 4 kW, 160 sccm Ar, 0.78 Pa, -200 V. Deposition parameters for HiPIMS: 4 kW, 0.65 Pa, 600 °C, -200 V, 40/1000 us.)

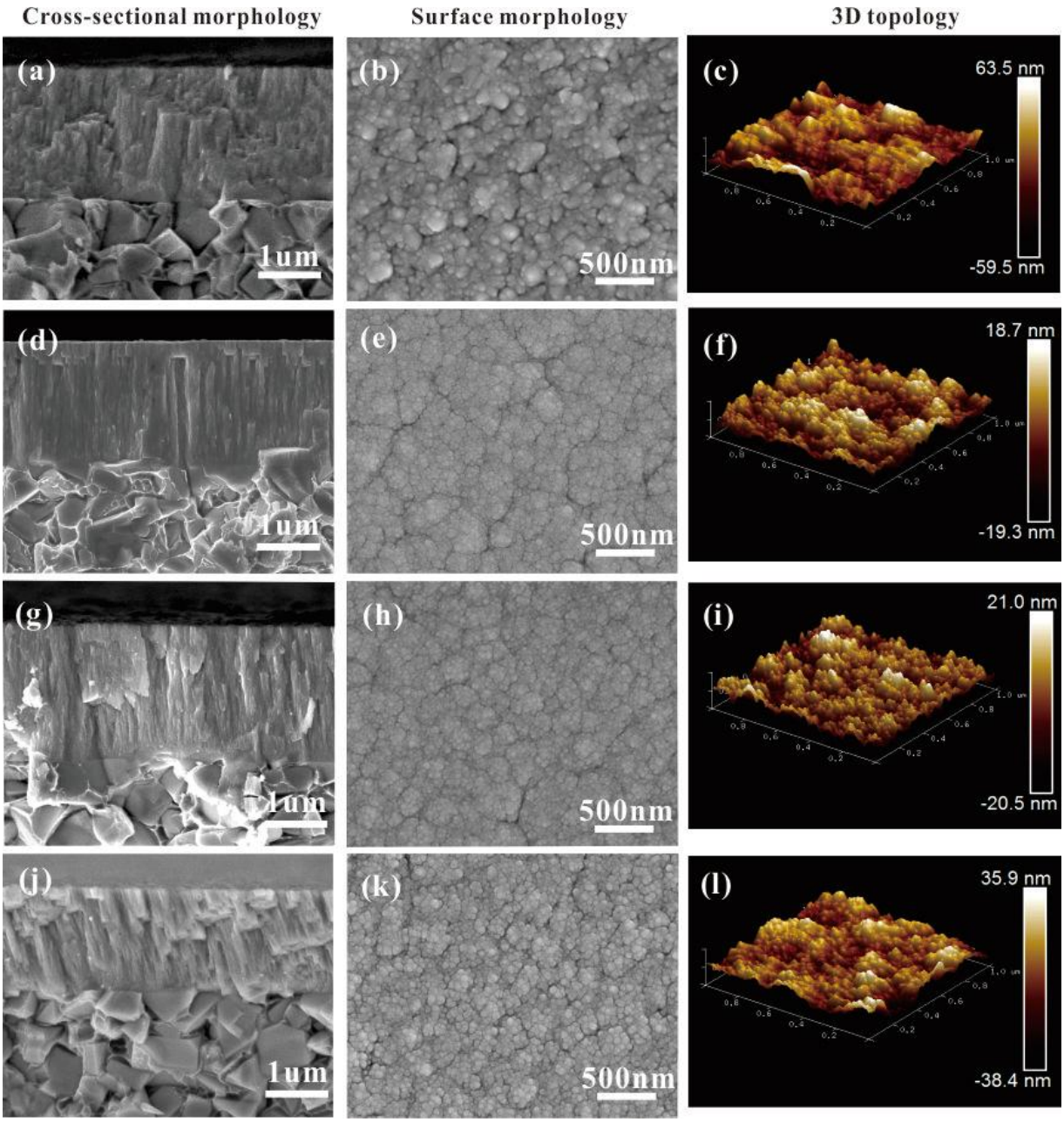

Fig. 4 Cross-sectional morphology, surface morphology and 3D topology of HfB_x coatings deposited by DCMS with different deposition conditions. (a-c) DC-1 sample; (d-f) DC-2 sample; (g-i) DC-3 sample; (j-l) DC-4 sample.

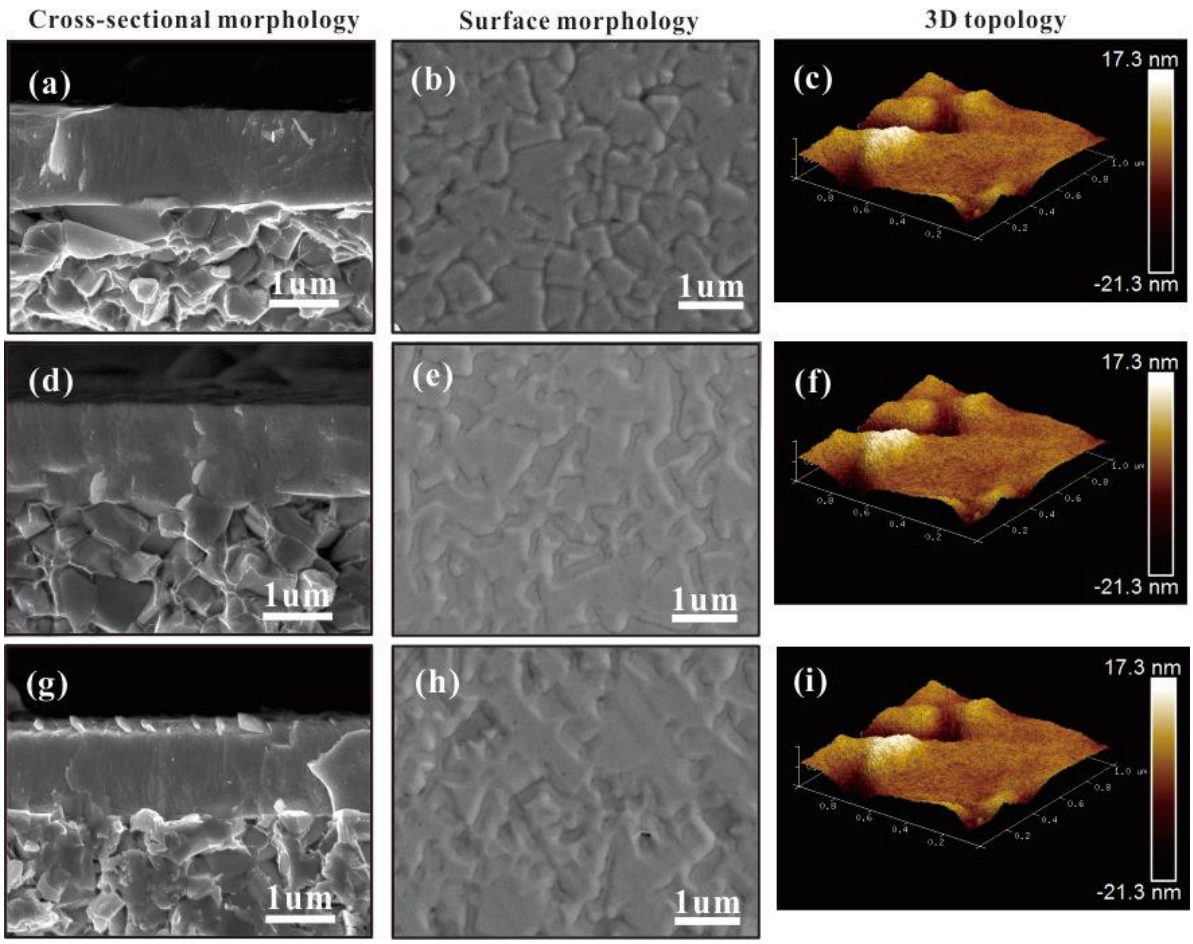

Fig. 5 Cross-section, surface morphology and 3D topology of HfB_x coating deposited by HiPIMS with different deposition conditions. (a-c) HiP-1 sample; (d-f) HiP-2 sample; (g-i) HiP-3 sample.

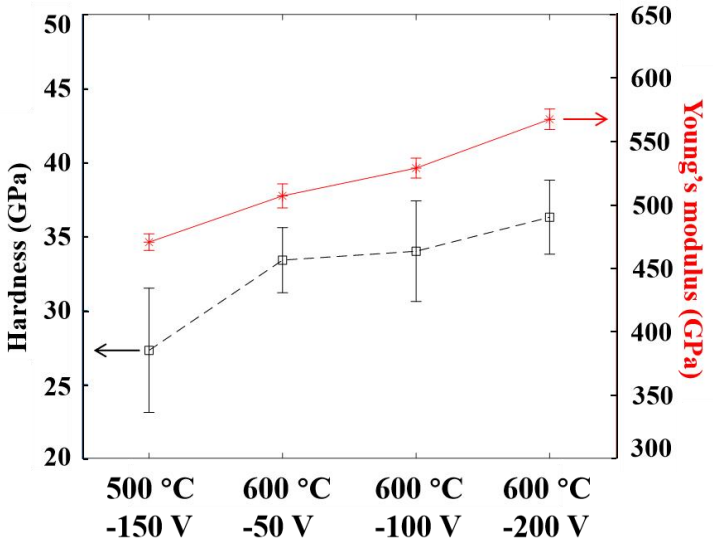

Fig. 6 Hardness and Young's modulus of HfB_x coating deposited by DCMS (Deposition parameters: 4 kW, 160 sccm Ar, 0.78 Pa.)

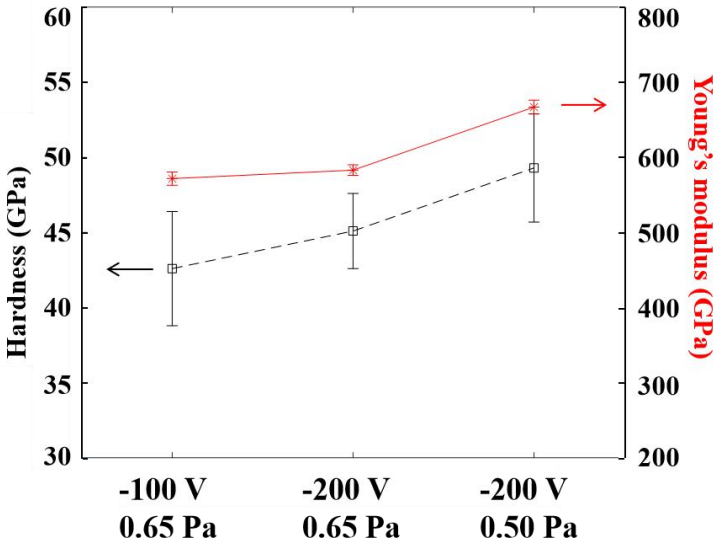

Fig. 7 Hardness and Young's modulus of HfB_x coating deposited by HiPIMS (Deposition parameters: 4 kW, 600 °C, 40/1000 us.)

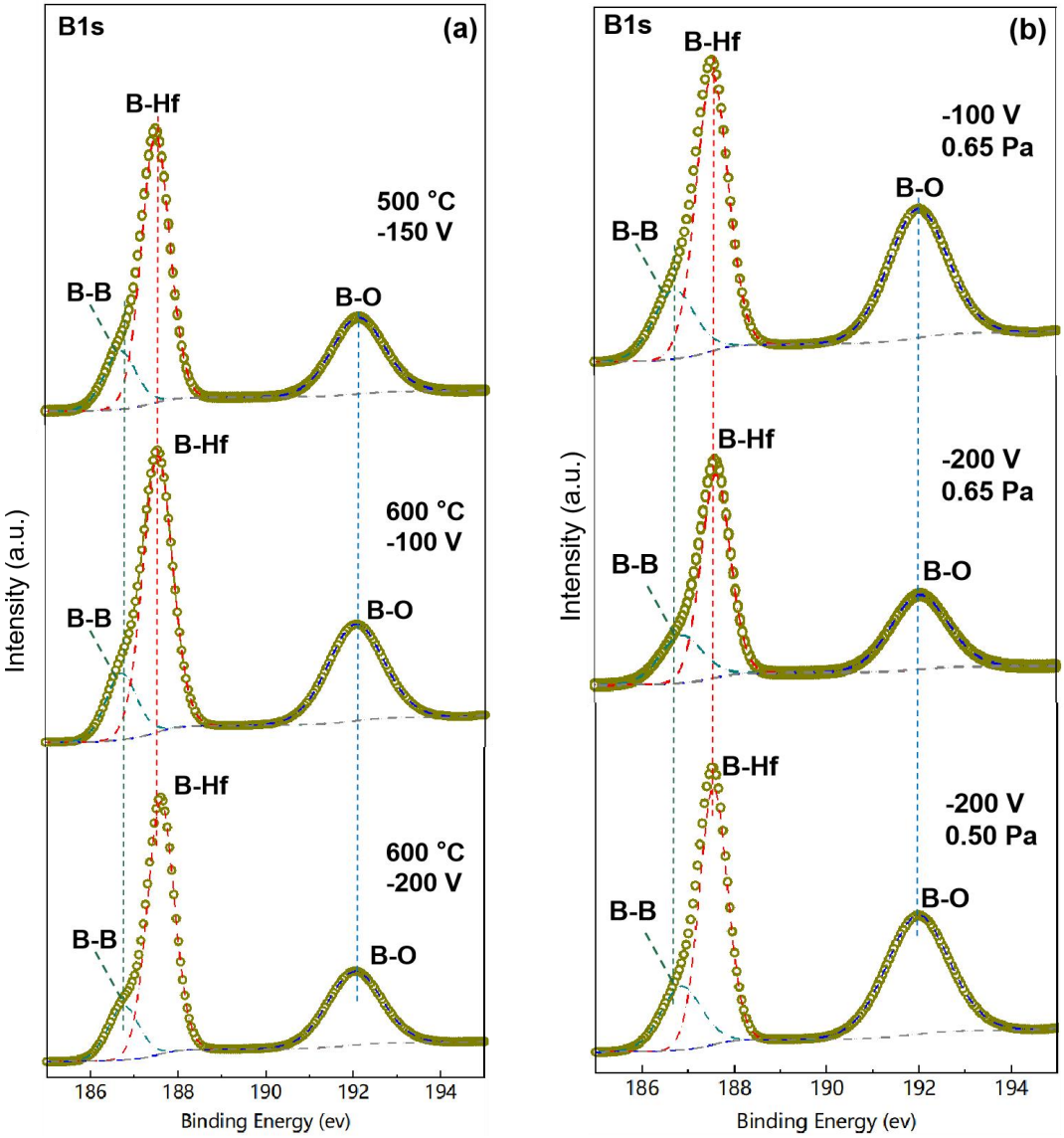

Fig. 8 High-resolution XPS B1s spectra of HfB_x coating deposited by (a) DCMS and (b) HiPIMS (deposition parameters for DCMS: 4 kW, 160 sccm Ar, 0.78 Pa. Deposition parameters for HiPIMS: 4 kW, 600 °C, 40/1000 us.)

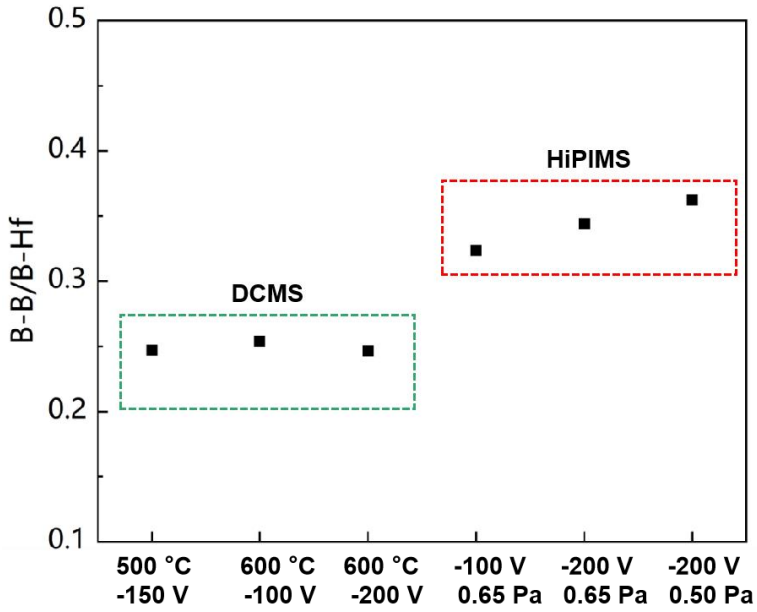

Fig. 9 The B-B/B-Hf ratios calculated from the area of B1s spectra from HfB_x coatings deposited by DCMS and HiPIMS (Deposition parameters for DCMS: 4 kW, 160 sccm Ar, 0.78 Pa, -200 V. Deposition parameters for HiPIMS: 4 kW, 0.65 Pa, 600 °C, -200 V, 40/1000 us)

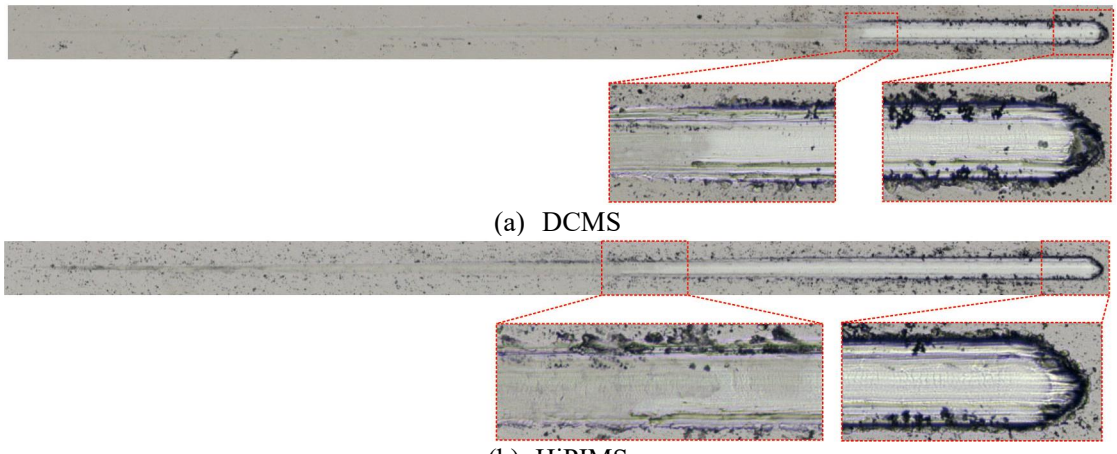

(a) DCMS

(b) HiPIMS

Fig. 10 Scratch test on the HfB_x coating deposited by (a) DCMS and (b) HiPIMS (Deposition parameters for DCMS: 4 kW, 160 sccm Ar, 0.78 Pa, -200 V. Deposition parameters for HiPIMS: 4 kW, 0.65 Pa, 600 °C, -200 V, 40/1000 us.)

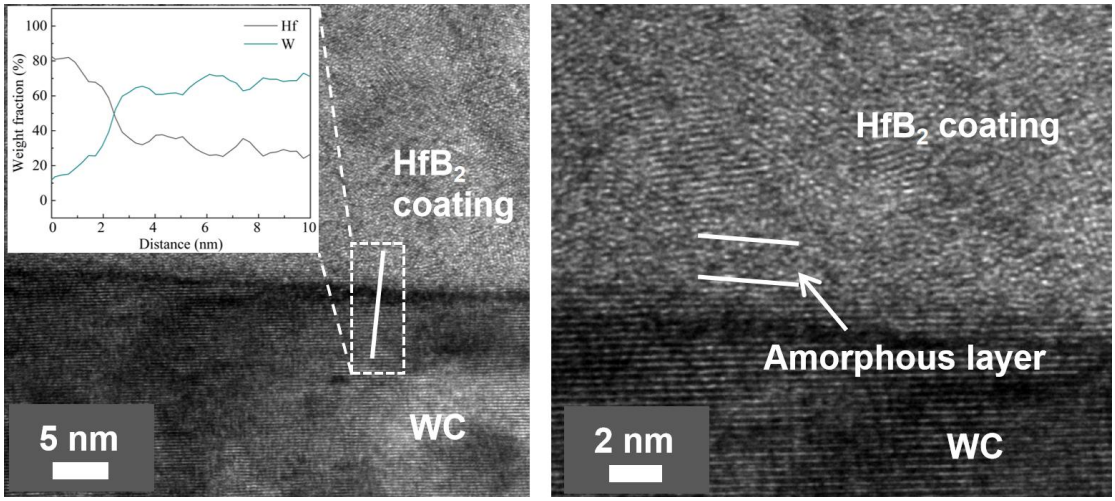

Fig. 11 The HRTEM images of the interface of the HfB_x coating and WC grains. (Deposition parameters: DCMS, 4 kW, 160 sccm Ar, 0.78 Pa, -200 V. The inset is a line-scan EDS signal scanned from the coating toward the substrate.)

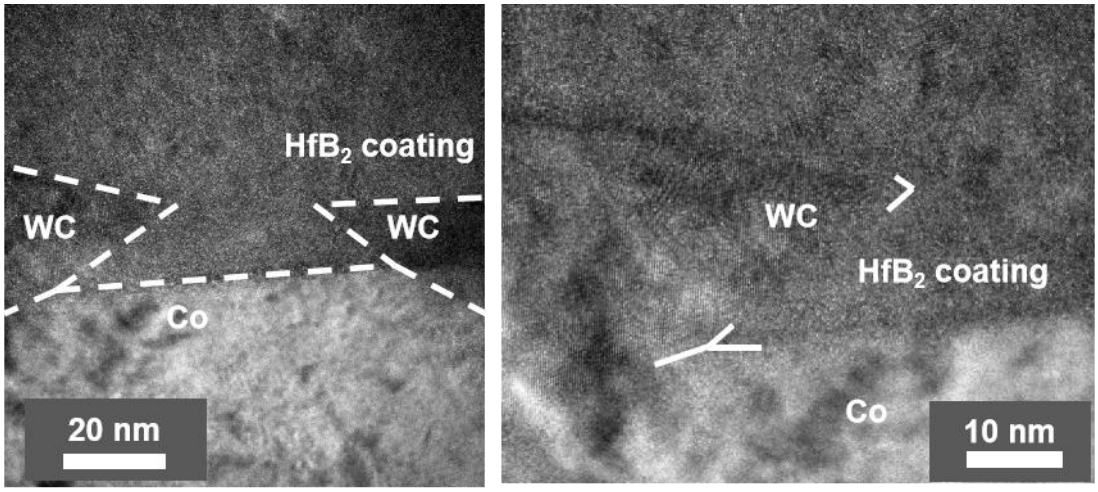

Fig. 12 The HRTEM images of the interface of the HfB_x coating and Co grains. (Deposition parameters: DCMS, 4 kW, 160 sccm Ar, 0.78 Pa, -200 V.)